Evidence for a high-pressure isostructural transition in nitrogen

Chunmei Fan
Sichuan University
Shan Liu
Sichuan University
Jingyi Liu
Sichuan University
Qiqi Tang
Sichuan University
Binbin Wu
Sichuan University
Yu Tao
Sichuan University
Meifang Pu
Sichuan University
Feng Zhang
Sichuan University
Jianfu Li
Linyi University
Xiaoli Wang
Yantai University
Duanwei He
Sichuan University
Li Lei (lei@scu.edu.cn)
Sichuan University https://orcid.org/0000-0002-8649-2928

Article

Keywords: diatomic molecules, high-pressure behaviors, nitrogen

Posted Date: November 17th, 2021

DOI: https://doi.org/10.21203/rs.3.rs-1019523/v1

Version of Record: A version of this preprint was published at Chinese Physics Letters on February 1st, 2022. See the published version at https://doi.org/10.1088/0256-307X/39/2/026401.

Abstract

Understanding the high-pressure behaviors of diatomic molecules (H_2, O_2, N_2, *etc*) is one of the most basic as well as important objective in high-pressure physics. Under high pressure diatomic molecule solids often exhibit rich crystal polymorphs. High-pressure isostructural transitions (HPIT) in solid hydrogen and oxygen, involving considerable technical challenges, have been experimentally documented, suggesting a possible prevailing pressure-driven molecular-symmetry breaking pathway. In spite of extensive efforts, however, HPIT in nitrogen has not been observed so far. Here we present a monoclinic-to-monoclinic isostructural phase transition ($\lambda \rightarrow \lambda'$) in solid nitrogen at approximately 50 GPa accompanied with anomalies in lattice parameter, atomic volume and Raman vibron modes. Further *ab initio* calculations strongly confirmed the HPIT in nitrogen, showing the weak distortion of orientation and slight rotation in nitrogen molecules possibly drive the low-pressure phase, λ-N_2, to an isostructural high-pressure phase, λ'-N_2 without changing crystal symmetry. In addition, we probed in detail the phase stability and revisited the pressure-temperature (P-T) phase diagram of nitrogen, discovering a new high-pressure amorphous phase, η'-N_2.

Introduction

High-pressure isostructural transition (HPIT) is identified with symmetrical invariance in structure, always signatured with volume collapse or the anomaly in axial ratios and phonon behavior. Although high-pressure experiments now reveal some key details about the behaviour of this transition, theoretical prediction is still exception challenging [1–12]. A typical HPIT has been observed in hexagonal-close-packed (hcp) structural metals, such as Cd [2], Zn [3, 4] and Os [5–7]. These transitions always accompanied with a discontinuous change of axial ratio c/a which was considered to be caused by the electronic topological transition (ETT), associated with a topological singularity of the Fermi surface induced by the distortion of the electronic band structure [2–7]. Metallic compounds, like CaB_4 [1] and MgB_2 [8], also have been discovered undergoing HPIT with a slope change in axial ratio c/a and the admitted explanation is the subtle change in the curvature of the electronic band dispersion near the Fermi surface within the Brillouin zone [1]. Besides, it has been demonstrated that molecular structural instability related to the rearrangement of hydrogen atoms can also lead to the occurrence of this phase transition (*e.g.*, H_2O [9], NH_3 [10], ND_3 [11]). Notably, the recent ultrahigh-pressure study reported a HPIT in solid hydrogen evidenced by a kink existing in the pressure dependence of unit cell parameter c, c/a ratio and volume, which probably caused by a highly distorted Brillouin zone and the breaking of molecular symmetry [12]. However, several doubts also raised. Firstly, the calculated electronic band structure of hydrogen at high density does not show any signal of ETT in the literature [12]. Besides, the pressure dependent c/a ratio presents a step drop in the experiments but calculations remain a stable increase without any anomaly using the predicted structure, suggesting the theoretical model ($P6_3/mmc$) may be unsuitable for the phase □ [12, 13].

In spite of the controversies in the solid hydrogen, it is the open question that inspired us to ask whether the HPIT could exist in other similar diatomic molecules solids. As simple homonuclear diatomic molecules, oxygen and nitrogen have similar properties with the hydrogen under sufficient high pressure, such as superconductivity and metallization [14–17]. Surprisingly, it has also been observed an isosymmetric phase transition from ε to ζ in solid oxygen, which is induced by atomic displacements [15, 16]. In fact, the behaviours of nitrogen at high density could be compared with hydrogen and oxygen. Owing to the strong N≡N covalent triple bonds, nitrogen becomes the most stable diatomic molecule and displays complex high-pressure behaviors [18–38]. Since the first report of nitrogen solids in the early last century, 20 solid nitrogen phases, at least, have been experimentally discovered in a wide area of pressures-temperatures (P-T) space, including solid-state molecular phases (α-N_2[19], β-N_2[20, 21], γ-N_2[22], δ-N_2[23], δ_{loc}-N_2[24, 25], ε-N_2[23], ζ-N_2[23, 26], ζ'-N_2[27], κ-N_2[28], θ-N_2[29], ι-N_2[30]and λ-N_2[30–32]), polymeric phases (cg-N[28], LP-N[33], HLPN[34], PLPN[35] and bp-N[36, 37]), an amorphous state (η-N_2[28, 38]) and a metallic phase[17]. A number of these phases perform significant regions of thermodynamic stability and others display thermodynamically metastable polymorphs but kinetically accessible [31]. Nevertheless, it is found that, up to now, no relevant studies have been reported on the HPIT in nitrogen with regard to experiments and calculations. As a high-pressure and low-temperature (HPLT) phase, λ-N_2 with a monoclinic structure, might be the most stable solid nitrogen [31–32, 39]. It was found that, formed by cold compression, once synthesized, the λ-N_2 can stabilize between 5-105 GPa at 77 K, and 30-150 GPa at 300 K, covering nine other ordinary phases in P-T space [25, 27]. Low formation enthalpy and unique lattice structure make the distinct phase unique and very stable. Whether the crystal structure of λ-N_2 could exhibit such stability? Is it possible to undergo a phase transition without changing symmetry (HPIT) in such a wide phase-stable space?

Therefore, the main purpose of this paper is to probe the phase stability in more detail and get clear structure information on the unique phase λ-N_2. In this work, we have conducted at least six independent high-pressure experiments along distinct P-T paths for probing the phase stability of λ-N_2 and revisited its phase diagram. The structural information of solid nitrogen (λ-N_2, δ-N_2, δ_{loc}-N_2 and ε-N_2) are measured by high-pressure angle dispersive X-ray diffraction (ADXRD) and high-pressure Raman scattering. *Ab initio* calculations are used for analyzing the structural properties and HPIT transition mechanism. The understanding of the nature of the HPIT in nitrogen could provide a better insight into the high-pressure behaviour on the linear diatomic molecules.

Results And Discussion

High-pressure isostructural transition in nitrogen. As shown in Fig. 1a, the main Bragg diffraction peaks of sample in the 10°-22° can be followed from 35.6 to 65.1 GPa, and all the peaks move towards a higher angle with the increasing pressure, indicating the decrease in lattice volume without significant structural phase transition. The diffraction peaks of gasket rhenium can be observed at higher pressures due to the shrinking of the sample cavity, and the intensity increase with the applied pressure. The pressure of the diffraction peaks calibrated by the gasket rhenium is close to the value measured with the high-frequency

edge of the first-order Raman mode of the diamond. Because of the preferred orientation of the solid molecular phase under pressure, diffraction peak along the (*h*00) direction can not be clearly discerned. The HPLT phase λ-N_2 was first discovered by Frost *et al*. [30], and a theoretical structure that previously predicted by Pickard and Needs [39] (space group $P2_1/c$; a= 2.922 Å, b= 2.891 Å, c= 5.588 Å and β = 132.54˚ for lattice parameters; x=0.5678, y=0.3764 and z=0.4534 for N atomic coordination at 40 GPa) was successfully used to fit the obtained experimental diffraction data. In this work, the structure given by Pickard and Needs [39] was also used for the initial model. Fig. 1b shows a excellent Rietveld refinement of data taken at 48.5 GPa (a= 2.908 Å, b= 2.869 Å, c= 5.367 Å and β = 131.87˚). However, our refinement results do exhibit abnormal discontinuous in the atomic volume (Fig. 2b) and β angle (Fig. 2c) at around 50 GPa, in conflict with our simulation parameter values with their structure which keeps decreasing in volume and increasing in β angle monotonically with the anisotropy increase under compression (Fig. 2a-c and Supplementary Fig. 1). We note that only 4 valid X-ray diffraction data, covering from 30 to 70 GPa, for λ-N_2 were given in the literature [30]. The reason why the discovery of the abnormal discontinuous in the structural parameters for λ-N_2 is more than 24 available diffraction data collected in the present work.

Thus, we reoptimized the crystal structure of λ-N_2 using VASP software. The calculations suggested that the monoclinic structure (space group $P2_1/c$) with atomic coordination (4*e*, x=0.0711; y=0.3720; z=0.4526) has higher enthalpy with the crystal structure in Ref. [39] below 50 GPa. Once the simulated external pressure of λ-N_2 exceeds 50 GPa (see Supplementary Fig. 5), both of the two structures have very similar enthalpy. The monoclinic structures with different coordination were plotted in Fig. 1c (Pickard *et al.*) and Fig. 1e (this work), respectively. Thus the obtained experimental XRD data are refined once again with the newly atomic positions calculated in this work and its reliability factor is better than the previous one. A representative Rietveld-refined diffraction picture at 55.4 GPa (a= 2.864 Å, b= 2.825 Å, c= 5.333 Å and β = 132.37˚) is displayed in Fig. 1d.

Figure 2b and Fig. 2c compared atomic volume and β angle of λ-N_2 at various pressure experimentally and theoretically. The lattice parameter β angle is the degree between the (002) and (100) planes. Associated with the structural instability of molecular solid and orientation of the local molecular pairs, the β angle is a key parameter to evaluate the behavior of solid nitrogen at high pressure. Without any change in the symmetry, the β angle exhibits significantly discontinuous compressive behaviors both in the experiment and theoretical calculation with the new atom positions (x=0.0711; y=0.3720; z=0.4526), indicating the occurrence of a unique structural transition. On the other hand, the volume of each nitrogen atom in λ phase does not decrease smoothly with increasing pressure, and a kink can be clearly observed at around 50 GPa (Figure 2b). The slope change in the P-V curve also underlining a discontinuity transition (Figure 2b). However, no signal of the anomaly on the P-V or P-β curve is observed with the previous structure (Pickard *et al.*) in the calculation. Combined the careful structural refinements with theoretical calculations, we prefer to think that a monoclinic-to-monoclinic isostructural transition occurs in the solid nitrogen, and the previously reported λ-N_2 should be indexed to as two different monoclinic

structures, the low-pressure phase λ-N_2 (the structure given by Pickard and Need [39]) and the high-pressure phase λ'-N_2 (the structure presented in this work).

The *P-V* relation on major molecular nitrogen phases is drawn in Fig. 2a. Our experimental data on λ-N_2, λ'-N_2, δ-N_2, δ_{loc}-N_2 and ε-N_2 are plotted and data from the literature (λ-N_2[30, 31], δ-N_2[23], δ_{loc}-N_2[24], ε-N_2[23, 26], ζ-N_2[26], κ-N_2[28]) are also shown for comparison. Further detailed work on δ-N_2, δ_{loc}-N_2 and ε-N_2 could be seen in Supplementary materials Fig. 3 and Fig. 4.

In order to probe the influence of lattice dynamics in the HPIT, the phonon spectra and phonon density of states (PDOS) of λ'-N_2 structure were calculated over the pressure range of 30 to70 GPa. As shown in Supplementary Fig. 6, the structure is dynamically stable up to 70 GPa, *i.e.* none of the phonon modes featured imaginary frequencies, the N≡N stretching modes were much higher in energy (from 2331 to 2497.5 cm^{-1}). No obvious change in phonon spectra and PDOS is observed. We plotted the band gap of λ-N_2 and λ'-N_2 as a function of pressure [Supplementary Fig. 7]. The electronic structure calculation showed that these phases are insulators, the insulating state is the result of the complete localization of valence electrons. In contrast to the pressure-induced isostructural electronic transitions in Os, Ce and H_2 *et al*., the HPIT in N_2 seems to have nothing to do with the change of phonon dispersion and electronic state.

Actually, λ-N_2 possesses the monoclinic structure and has a flexible β angle. And its space group, $P2_1/c$, is based on an fcc lattice, but with molecular displacements and a significant cell distortion. There are two diatomic polarized molecular pairs with different orientations in the unit cell. The blue molecular pairs in the edges of the unit cell are parallel to each other, whereas the red ones are in the center of the structure. It is to be expected that along the isotherm the orientation effect is weaker than the configuration effect at high densities. Hence, the unite cell parameters *a*, *b* and *c* are decreasing and the β angle is increasing under compression. However, the orientation stability of the polarized molecular pairs is prone to be distorted and the β angle is easier to be damaged at higher pressure (> 50 GPa). In addition, the vibration-rotation coupling (VRC) [40] also exists in solid nitrogen. Besides, medium pressure is a node of the *van der Waals* bond and the N≡N covalent bond in the nitrogen molecules. At low to moderate pressure (approximately 5 to 50 GPa), the electronic quadrupole-quadrupole interaction between nitrogen molecules increases sharply as intermolecular distances decrease under compressing. Whereas the electrons' energy surpasses the electrostatic potential energy above 50 GPa, part of molecules' triple bond electronic density is shifted to intermolecular regions, leading to the weakening of N≡N intramolecular triple bond [37]. In the case of the ordinary phase via regular room-temperature compression path, it is occurred that the structural phase transition from ε-N_2 to ζ-N_2 at about 56 GPa because of the change of interaction in nitrogen molecules [41]. Based on a combination of the above reasons, the nitrogen atoms rearrange and orientation change under extreme stain environment with the increasing anisotropy, indicating an isostructural phase transition from λ-N_2 to λ'-N_2, associating with the molecular-symmetry breaking.

The phase of λ'-N_2 was originally observed on the basis of anomaly in Raman spectra. Fig. 3a displays the typical Raman spectra of λ-N_2 (λ'-N_2) at room temperature and the subtle variation of high-frequency Raman shift *verse* pressure is depicted in Fig. 3b. The complete Raman peaks of the λ-N_2 (λ'-N_2) at various pressure could be seen in supplementary materials Fig. 2. λ-N_2 has seven Raman active optical modes. As shown in Fig. 3c, the low-frequency lattice phonon modes ($A_g^{(1)}$, $B_g^{(1)}$, $A_g^{(2)}$, $B_g^{(2)}$) are related to the motion between nitrogen molecules (van der Waals force) and high-frequency vibron modes ($A_g^{(3)}$ and $B_g^{(3)}$) are connected with the linear symmetrical tensile vibrations of atoms within a molecule (force of the covalent bond). The emergence of A_g', a disorder-activated Raman mode, is due to the broken space translation symmetry by limited size, elemental doping, local strain and fluctuations induced by thermodynamic factors [32]. From our experiments, three high-frequency modes show discontinuous changes in adjacent pressures. Slight kinks are emerged in $A_g^{(3)}$ and $B_g^{(3)}$ around 49 GPa and 46 GPa, respectively. What is more, the strongest vibration mode, $A_g^{(3)}$, gets the maximum frequency (2393.5 cm^{-1}) and then performs a sudden anomalous softening behavior at about 55 GPa. It is likely that different lattice vibration modes have distinct responses to the compression.

The phase stability and revisited diagram of λ-N_2. In this work, we also probed the phase stability of λ-N_2 (λ'-N_2). The transformation and phase diagram of nitrogen is shown in Fig. 4, six independent *P-T* paths via compression at 77 K up to at least 35, 36, 55, 61, 115 and 117 GPa are exhibited, which further refined the thermodynamic region of λ-N_2 and λ'-N_2. The former *P-T* space of λ-N_2 in Ref 32. should be divided into two parts, a lower-pressure region for the λ-N_2 and a higher-pressure region for the λ'-N_2. Contrasted with the previous work, our finding shows that the λ'-N_2 can stabilize up to at least 176 GPa at room temperature accompanied with the broaden and weaken of Raman peaks (Fig. 5b). When external load exceeds 178 GPa, all Raman peaks of λ'-N_2 disappeared and the sample was completely became opaque. It is also the highest pressure that molecular nitrogen phases could exist up to now. Once gained the target nitrogen phase, cooled it to 77 K and 64 GPa, we found out that λ'-N_2 and ζ-N_2 can coexist at the same *P-T* condition (seen in Fig. 5d). Therefore, the low-temperature (77 K) boundary between λ'-N_2 and ζ-N_2 should be down to 64 GPa, which is much lower than the previously reported 107 GPa in Ref.32. It is noteworthy that the coexistence phase (λ'-N_2 and ζ-N_2) was also observed in the 115 GPa and 300 K (Fig. 5f). Thus, it means that the sample goes into a metastable region above 64 GPa and could continually keep up to 115 GPa at low temperature. What is more, loading purity liquid nitrogen more than 117 GPa at 77 K and a new high-pressure nitrogen phase, referred to as η'-N_2, with significant inactivation in Raman bands was formed (Fig. 5f). It has not been verified whether η'-N_2 belongs to an amorphous phase like η-N_2. The reported amorphous η-N_2 can be obtained around 140 GPa at 300 K and has a large hysteresis, accompanied with the disappearance of the Raman signal and the emergence of a measurable resistance [27, 28]. And the transition condition from molecular to nonmolecular phase could shift to a higher pressure when decreasing temperature. Differ from the synthetic condition of the η-N_2, the η'-N_2 is easier to access at a lower pressure and room temperature via λ'-N_2 transforming probably owing to minimizing the energetic barriers with the unique structure.

After the hydrogen and oxygen, the HPIT has also been observed in nitrogen, which allow us to think that the transition associated with molecular-symmetry breaking is a common phenomenon in diatomic molecules under high pressure, even difference in the transition mechanisms, it is an indispensable step toward the dissociation and metallization.

Conclusion

In summary, the formation conditions, phase stabilization, structural property and *P-V* compression curve of λ-N_2 (λ'-N_2) have been carefully discussed. A pressure-induced monoclinic-to-monoclinic isostructural phase transition has been confirmed by high-pressure X-ray diffraction, high-pressure Raman scattering experiments and theoretical calculations. The transition is possibly caused by the coupling of distorted orientation and rotation in nitrogen molecules associating with molecular-symmetry breaking.

Methods

Experiments

Sample preparation. High-pressure was generated using a symmetric-type diamond anvil cell (DAC) with 100~300 μm culets. Rhenium was used as the gasket material precompressed to 10-30 μm thickness with a sample chamber drilled using 1064 nm laser cutting to produce 30-100 μm diameter holes. Our samples were successfully synthesized by compression of purity liquid (77 K) and then warmed to ambient temperature (300 K) for Raman and *in situ* ADXRD experiments.

Sample measurements. High-pressure Raman scattering experiments were carried out using a custom-built confocal Raman spectrometry system in the back-scattering geometry based on Andor Shamrock triple grating monochromator with an attached ANDOR Newton EMCCD, excitation by a solid-state laser at 532 nm, and collection by a 20× Mitutoyo objective. Considering ruby fluorescence scale method for the high pressure above 100 GPa cannot be read accurately, we only adopt the first-order diamond phonon [42, 43] as pressure calibration in the high-pressure Raman experiments.

Synchrotron radiation experiment was performed after the synthesis of the target samples (λ-N_2) confirmed by Raman measurements. The ADXRD data on λ-N_2 was collected at the BL15U1 beam line of the Shanghai Synchrotron Radiation Facility (SSRF, China) and the X-ray beam down to about 2.5×2.5 μm^2 with 0.6199Å wavelength. Pressures on the sample were measured using the high-frequency edge of the diamond phonon[42, 43]. Another ADXRD experiment (δ-N_2, δ_{loc}-N_2, ε-N_2) was carried out in the 4W2 beam line of the Beijing Synchrotron Radiation Facility (BSRF, China). A Si (111) monochromator was used to tune the synchrotron source with a wavelength of 0.6199 Å and the incident X-ray beam was focused to approximately 20×30 μm^2 full width. The pressure was detected by the ruby fluorescence method [44] and the EOS of Re [45]. The measured pressure error which used the two methods is within 0.5 GPa. The two-dimensional diffraction patterns were analyzed with the programs Dioptas [46] and

Fit2D [47], respectively. The structural refinements were performed by using software GSAS to get the lattice parameters [48].

Calculations The structures mentioned here were searched by the swarm intelligence CALYPSO method [49, 50]. The total energy calculations and structure optimization were carried out using the plane wave basis, projected augmented wave (PAW) potentials, and generalized gradient approximation (GGA) with the Perdew-Burke Ernzerh (PBE) of exchange-correlation functional as implemented in the Vienna ab initio simulation package (VASP) [51–55]. The frozen-core all electron PAW potentials were used with $2S^2 2P^3$ treated as valence electrons for N. The Van der Waals density functional, namely optB86b-vdW, was adopted to treat dispersion forces. The cutoff energy (900 eV) for the expansion of the wave function into plane waves and Monkhorst-Pack [56] *k*-meshes (*k*-points density 0.02 $Å^{-1}$) are chosen to ensure that all the enthalpy calculations are well converged to better than 1 meV/atom. Using CALYPSO, we searched the structures of nitrogen with simulation cell sizes of 1-40 formula units (f.u.) in the pressure range of 0-60 GPa. As shown in Fig. 1(e), our structure simulations uncovered a monoclinic phase (space group: $P2_1/c$) at 60 GPa, which is consistent with our experiment. Phonon calculations were performed on the structures to determine their dynamic stability, by using a finite displacement approach as per the PHONOPY code [57, 58].

Data availability

All relevant data sets generated and/or analysed during this study are available from the corresponding author upon reasonable request.

Declarations

Acknowledgments

We acknowledge financial support from the National Natural Science Foundation of China (Grant No. 11774247, U2030107 and 11974154), Sichuan University Innovation Research Program of China (No. 2020SCUNL107), Chinese Academy of Sciences (Grant No. 2019-BEPC-PT-003237) and Natural Science Foundation of Shandong Province (Grant Nos. 2019GGX103023 and Z2018S008).

Author contributions

L. L. conceived the project. X. W. performed the numerical calculations. C. F., S. L., J. L. and L. L. performed the experiments. L. L., C. F. and X. W. wrote this paper. All authors discussed and interpreted the results.

Competing interests

The authors declare no competing interests.

References

1. Li, G. et al. Pressure-induced isostructural phase transition in CaB_4. *RSC Adv.* **4**, 42523–42529 (2014).
2. Pratesi, G., Cicco, A. D., Minicucci, M. & Itiè, J-P. Anomalies in the structure of solid Cd under pressure: an x-ray diffraction study. *J. Phys.*: *Condens. Matter* **17**, 2625–2632 (2005).
3. Li, Z. & Tse, J. S. Phonon anomaly in high-pressure Zn. *Phys. Rev. Lett.* **85**, 5130–5133 (2000).
4. Kechin, V. V. Electronic topological transitions in Zn under compression. *Phys. Rev. B* **63**, (2001).
5. Occelli, F. et al. Experimental evidence for a high-pressure isostructural phase transition in osmium. *Phys. Rev. Lett.* **93**, 095502 (2004).
6. Ma, Y., Cui, T., Zhang, L., Xie, Y. & Zou, G. Electronic and crystal structures of osmium under high pressure. *Phys. Rev. B* **72**, 174013 (2005).
7. Dubrovinsky, L. et al. The most incompressible metal osmium at static pressures above 750 gigapascals. *Nature* **525**, 226–229 (2015).
8. Sun, L., Kikegawa, T., Wu, Q., Zhan, Z. & Wang, W. Isostructural transition of MgB_2 under high pressure. *Chin. Phys. Lett.* **18**. 1401–1403 (2001).
9. Queyroux, J.-A. et al. Melting curve and isostructural solid transition in superionic ice. *Phys. Rev. Lett.* **125**, 195501 (2020).
10. Datchi, F. et al. Solid ammonia at high pressure: a single-crystal x-ray diffraction study to123 GPa. *Phys. Rev. B* **73**, 174111 (2006).
11. Ninet, S. et al. Hydrogen bonding in ND_3 probed by neutron diffraction to 24 GPa. *Phys. Rev. B* **79**, 100101(R) (2009).
12. Ji, C. et al. Ultrahigh-pressure isostructural electronic transitions in hydrogen. *Nature* **573**, 558–562 (2019).
13. Ackland, G. J. & Loveday, J. S. Structures of solid hydrogen at 300 K. *Phys. Rev. B* **101**, 094104 (2020).
14. Loubeyre, P., Occelli, F. & Dumas, P. Synchrotron infrared spectroscopic evidence of the probable transition to metal hydrogen. *Nature* **577**, 631–635 (2020).
15. Akahama, Y., Kawamura, H., Hausermann, D., Hanfland, M. & Shimomura, O. New high-pressure structural transition of oxygen at 96 GPa associated with metallization in a molecular solid. *Phys. Rev. Lett.* **74**, 4690–4693 (1995).
16. Freiman, Y. A., Jodl, H. J. & Crespo, Y. Solid oxygen revisited. *Phys. Rep.* **743**, 1–55 (2018).
17. Jiang, S. et al. Metallization and molecular dissociation of dense fluid nitrogen. *Nat. Commun.* **9**, 2624 (2018).
18. Wang, X. et al. Cagelike diamondoid nitrogen at high pressures. *Phys. Rev. Lett.* **109**, 175502 (2012).
19. Schuch, A. F. & Mills, R. L. Crystal structures of the three modifications of nitrogen 14 and nitrogen 15 at high Pressure. *J. Chem. Phys.* **52**, 6000–6008 (1970).

20. Streib, W. E., Jordan, T. H. & Lipscomb, W. N. Single-crystal X-ray diffraction study of β nitrogen. *J. Chem. Phys.* **37**, 2962–2965 (1962).
21. Zinn, A. S., Schiferl, D. S. & Nicol, M. F. Raman spectroscopy and melting of nitrogen between 290 and 900 K and 2.3 and 18 GPa. *J. Chem. Phys.* **87**, 1267–1271 (1987).
22. Mills, R. L. & Schuch, A. F. Crystal structure of gamma nitrogen*. *Phys. Rev. Lett.* **23** 1154–1156 (1969).
23. Olijnyk, H. High pressure x-ray diffraction studies on solid N_2 up to 43.9 GPa. *J. Chem. Phys.* **93**, 8968–8972 (1990).
24. Stinton, G. W., Loa, I., Lundegaard, L. F. & McMahon, M. I. The crystal structures of δ and δ* nitrogen. *J. Chem. Phys.* **131**, 104511 (2009).
25. Hanfland, M., Lorenzen, M., Wassilew-Reul, C. & Zontone, F. Structures of molecular nitrogen at high pressures. *Rev. High Pressure Sci. Technol.* **7** 787–789 (1998).
26. Eremets, M. I. et al. Structural transformation of molecular nitrogen to a single-bonded atomic state at high pressures. *J. Chem. Phys.* **121**, 11296–11300 (2004).
27. Gregoryanz, E., Goncharov, A. F., Hemley R. J. & Mao, H.-K. High-pressure amorphous nitrogen. *Phys. Rev. B* **64**, 052103 (2001).
28. Gregoryanz, E. et al. High *P-T* transformations of nitrogen to 170 GPa. *J. Chem. Phys.* **126**, 184505 (2007).6
29. Gregoryanz, E. Raman, infrared, and x-ray evidence for new phases of nitrogen at high pressures and temperatures. *Phys. Rev. B* **66**, 224108 (2002).
30. Frost, M., Howie, R. T., Dalladay-Simpson, P., Goncharov, A. F., & Gregoryanz, E. Novel high-pressure nitrogen phase formed by compression at low temperature. *Phys. Rev. B* **93** 024113 (2016).
31. Sontising, W., & Beran, G. J. Theoretical assessment of the structure and stability of the λ phase of nitrogen. *Phys. Rev. Mater.* **3**, 095002 (2019).
32. Liu, S. et al. Raman spectroscopy and phase stability of λ-N_2. *Solid State Commun.* **310**, 113843 (2020).
33. Ma Y., Oganov, A. R., Li, Z., Xie, Y., & Kotakoski, J. Novel high pressure structures of polymeric nitrogen. *Phys. Rev. Lett.* **102**, 065501 (2009).
34. Laniel, D., Geneste, G., Weck, G., Mezouar, M. & Loubeyre, P. Hexagonal layered polymeric nitrogen phase synthesized near 250 GPa. *Phys. Rev. Lett.* **122**, 066001 (2019).
35. Lei, L. et al. Evidence for a new extended solid of nitrogen. *Chin. Phys. Lett.* **37**, 068101 (2020).
36. Ji, C. et al. Nitrogen in black phosphorus structure. *Sci. Adv.* **6**:eaba9206 (2020).
37. Laniel, D. et al. High-pressure polymeric nitrogen allotrope with the black phosphorus structure. *Phys. Rev. Lett.* **124**, 216001 (2020).
38. Eremets, M. I., Hemley, R. J., Mao, H.-K. & Gregoryanz, E. Semiconducting non-molecular nitrogen up to 240 GPa and its low-pressure stability. *Nature* **411** (2001).

39. Pickard, C. J., & Needs, R. J. High-pressure phases of nitrogen. *Phys. Rev. Lett.* **102**, 125702 (2009).
40. Scheerboom, M. I. M. & Schouten, J. A. Anomalous behavior of the vibrational spectrum of the high-pressure δ phase of nitrogen: a second-order transition. *Phys. Rev. Lett.* **71**, 2252–2255 (1993).
41. Pu, M. et al. Raman study of pressure-induced dissociative transitions in nitrogen. *Solid State Commun.* **298**, 113645 (2019).
42. Akahama, Y., & Kawamura, H. High-pressure Raman spectroscopy of diamond anvils to 250 GPa: method for pressure determination in the multimegabar pressure range. *J. Appl. Phys.* **96**, 3748–3751 (2004).
43. Akahama, Y., & Kawamura, H. Pressure calibration of diamond anvil Raman gauge to 410 GPa. *J. Phys. Conf. Ser.* **215**, 012195 (2010).
44. Mao, H. K., Xu, J. & Bell, P. M. Calibration of the ruby pressure gauge to 800 kbar under quasi-hydrostatic conditions. *J. Geophys. Res.* **91**, 4673 (1986).
45. Zha, C-S., Bassett, W. A. & Shim, S-H. Rhenium, an in situ pressure calibrant for internally heated diamond anvil cells. *Rev. Sci. Instrum.* **75**, 2409–2418 (2004).
46. Prescher, C. & Prakapenka, V. B. DIOPTAS: a program for reduction of two-dimensional X-ray diffraction data and data exploration. *High Pressure Res.* **35**, 223–230 (2015).
47. Hammersley, A. P., Svensson, S. O., Hanfland, M., Fitch, A. N. & Hausermann, D. Two-dimensional detector software: from real detector to idealised image or two-theta scan. *High Pressure Res.* **14**, 235–248 (1996).
48. Toby, B. H. EXPGUI, a graphical user interface for GSAS. *J. Appl. Crystallogr.* **34**, 210–213 (2001).
49. Lv, J., Wang ,Y., Zhu, L. & Ma, Y. Predicted novel high-pressure phases of lithium. *Phys. Rev. Lett.* **106**, 015503 (2011).
50. Wang, Y., Lv, J., Zhu, L. & Ma, Y. Crystal structure prediction via particle-swarm optimization. *Phys. Rev. B* **82**, 094116 (2010).
51. Kresse, G. & Furthmüller, J. Efficient iterative schemes for *ab initio* total-energy calculations using a plane-wave basis set. *Phys. Rev. B* **54**, 11169–11186 (1996).
52. Kresse, G. & Joubert, D. From ultrasoft pseudopotentials to the projector augmented-wave method. *Phys. Rev. B* **59**, 1758–1775 (1999).
53. Dong, W., Kresse, G., Furthmüller, J. & Hafner, J. Chemisorption of H on Pd(111) An *ab initio* approach with ultrasoft pseudopotentials. *Phys. Rev. B* **54**, 2157–2166 (1996)
54. Blochl, P. E. Projector augmented-wave method. *Phys. Rev. B* **50**, 17953–17979 (1994).
55. Perdew, J. P., Burke, K., & Ernzerhof, M. Generalized gradient approximation made simple. *Phys. Rev. Lett.* **77**, 3865–3868 (1996)
56. Monkhorst, H. J. & Pack, J. D. Special points for Brillouin-zone integrations. *Phys. Rev. B* **13**, 5188–5192 (1976).
57. Togo, A., Oba, F. & Tanaka, I. First-principles calculations of the ferroelastic transition between rutile-type and $CaCl_2$-type SiO_2 at high pressures. *Phys. Rev. B* **78**, 134106 (2008).

58. The force constants matrix is determined by VASP. Convergence test gave the use of a 3 x 3 x 2 supercell.

Figures

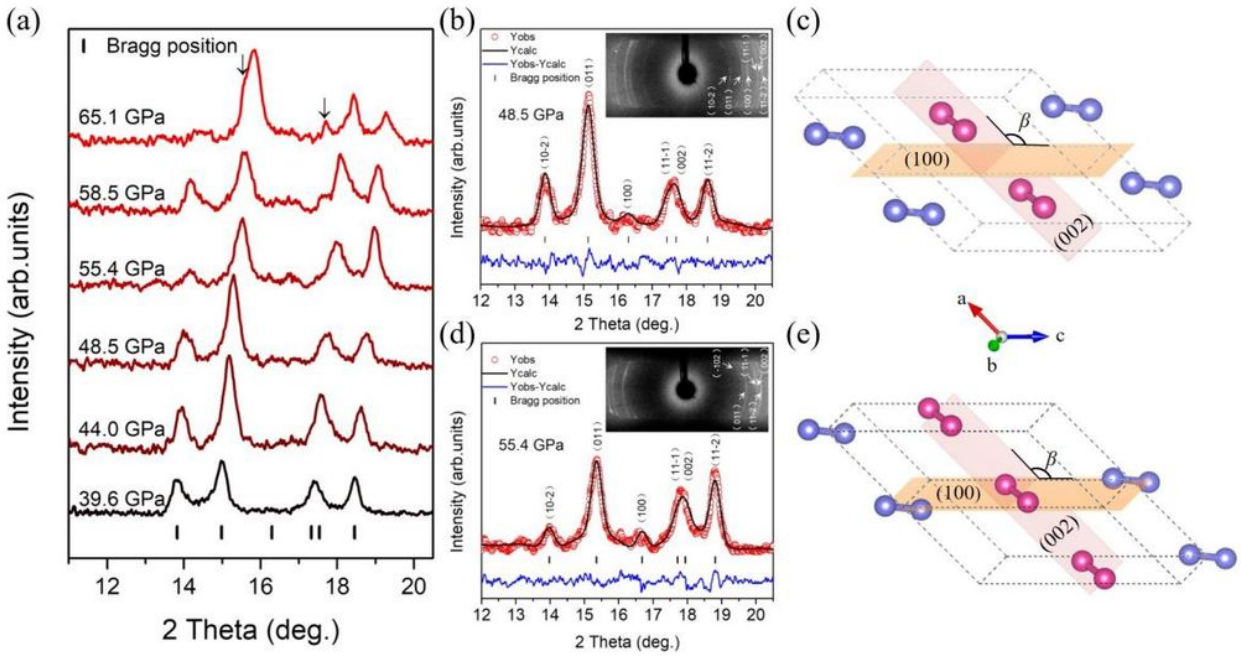

Figure 1

X-ray diffraction data and structure information of λ-N2 (λ'-N2). a X-ray diffraction patterns with the wavelength of 0.6199 Å on room-temperature compression. The arrows are marked the diffraction peaks of gasket rhenium. Representative Rietveld-refined diffraction patterns with the corresponding unintegrated patterns for the b λ-N2 at 48.5 GPa and d for the λ'-N2 at 55.4 GPa. c The crystal structure of λ-N2 with atomic position predicted by Pickard and Needs [39] (x=0.5678; y=0.3764; z=0.4534). e The crystal structure of λ'-N2 with new nitrogen atom coordination (x=0.0711; y=0.3720; z=0.4526).

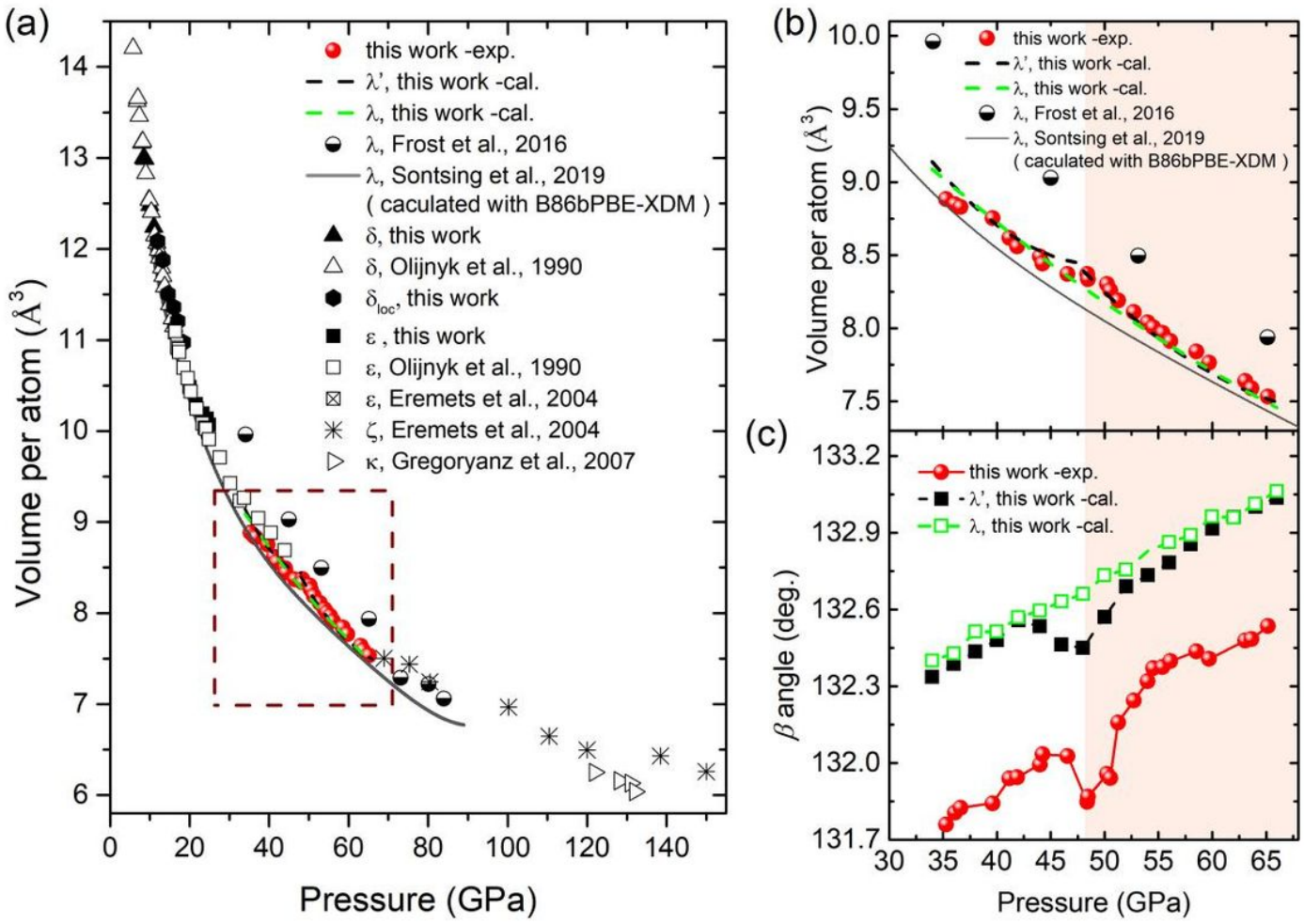

Figure 2

Structural parameters of solid nitrogen under high pressure. a The P-V compression curves for the major molecular nitrogen phases. Solid shapes represent the present experimental data for λ-N2, λ'-N2, δ-N2, δloc-N2 and ε-N2. The black and green dash lines represent our calculation data for λ-N2 and λ'-N2, respectively. Data from the literature are also shown for comparison, λ-N2[30,31], δ-N2[23], δloc-N2[24], ε-N2[23, 26], ζ-N2[26], κ-N2[28]. b The detailed area of the red frame is in the Fig. 2a. c The pressure dependence of β angle for the λ-N2 and λ'-N2, the white and light red sections correspond to phase region of λ-N2 and λ'-N2, respectively.

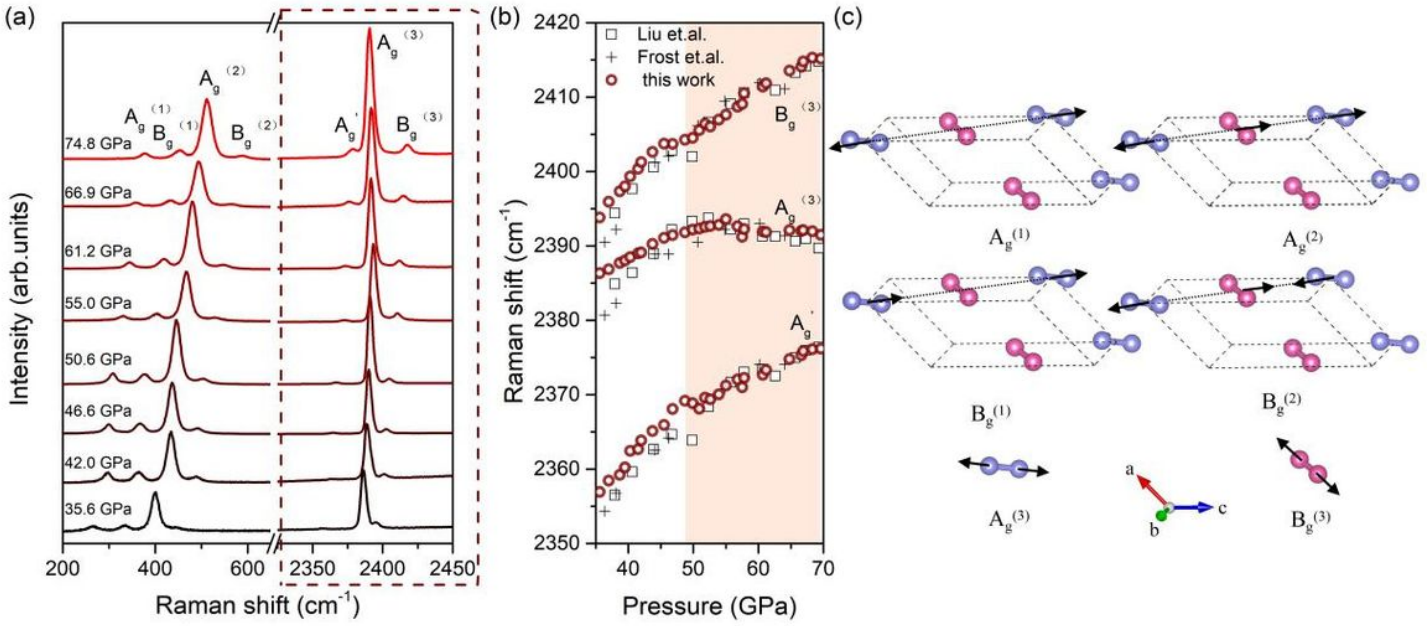

Figure 3

Raman data for the λ-N2 (λ’-N2). a Representative Raman spectra of λ-N2 (λ’-N2) on room-temperature compression. b High-frequency Raman peaks of the λ-N2 (λ’-N2) as a function of pressure at ambient temperature in experiments. The red circles are the present work. The hollow squares and vertical crosses are previous experiments data[30, 32]. c The atomic displacements diagram of λ’-N2 including the Ag(1), Ag(2), Bg(1), Bg(2), Bg(3) and Bg(3) modes.

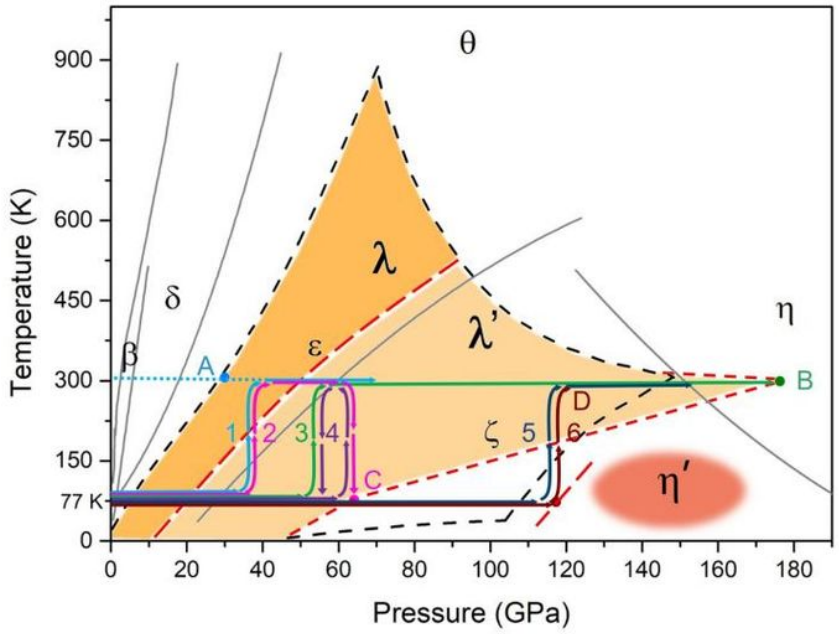

Figure 4

Transformation and phase diagram of nitrogen. The deep orange section and lighter section are the forming region of λ-N2 and λ'-N2, respectively. The red section is the region of η'-N2. Six colorful lines are different P-T paths to explore λ-N2 and λ'-N2 formation and transition. The red dashed lines represent the revised transition boundaries of λ-N2 and λ'-N2. The black dashed lines show the boundaries of λ-N2 in Ref.[30,32]. The gray lines show the phase boundaries of nitrogen previously observed under compression at room temperature.

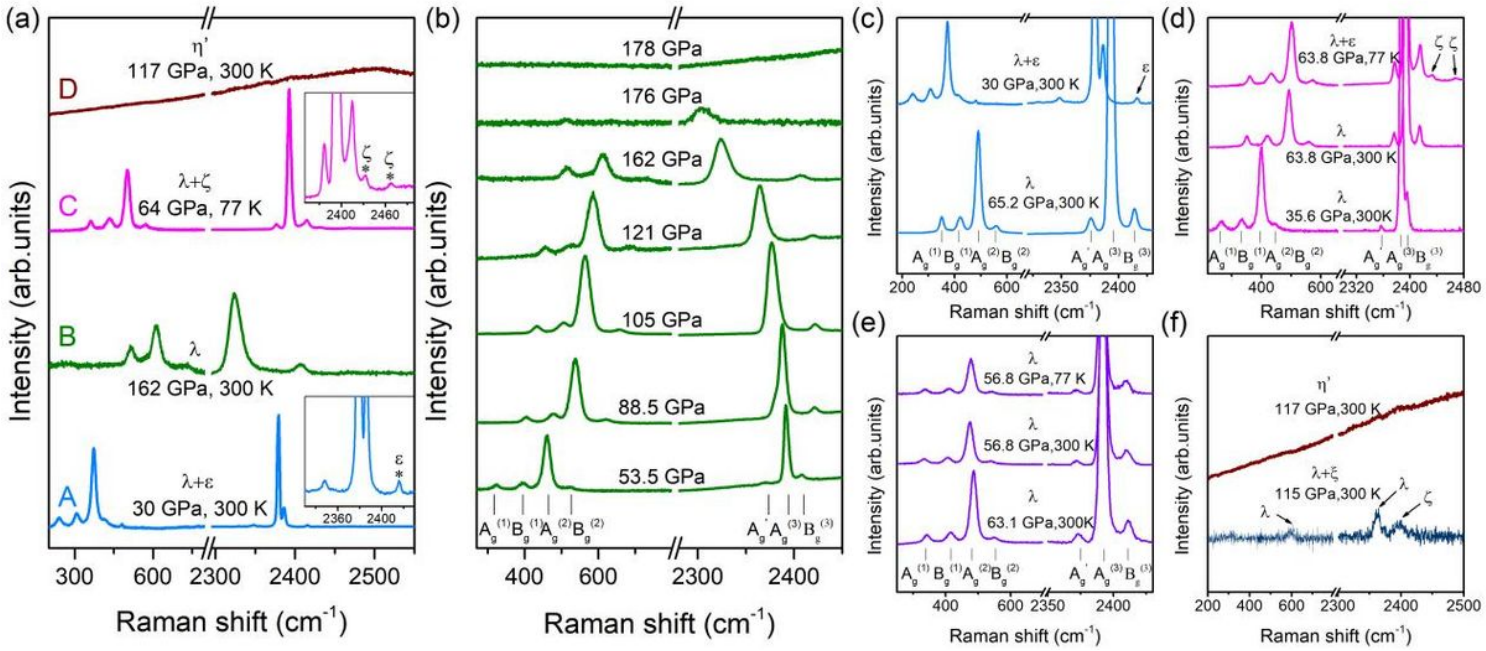

Figure 5

The Raman spectra correspond to the P-T points and paths in the Fig. 4. a The corresponding P-T points for A, B, C and D, along b the path 3, c path 1, d path 2, e path 4, f paths 5 (upper) and 6 (lower).

Supplementary Files

This is a list of supplementary files associated with this preprint. Click to download.

- SupplementaryInformation.docx